Persistence of strong correlations in the energy spectrum of a separable Hamiltonian system: The rectangular box

J. M. A. S. P. Wickramasinghe, B. Goodman, and R. A. Serota
Department of Physics, University of Cincinnati, Cincinnati, Ohio 45221-0011, USA
(Received 23 August 2004; published 15 November 2005)

The variance of the number of levels in an energy interval around a level with large quantum numbers (semiclassical quantization) is studied for a particle in a rectangular box. Sampling involves changing the ratio of the rectangle's sides while keeping the area constant. For sufficiently narrow intervals, one finds the usual linear growth with the width of the interval. For wider intervals, the variance undergoes large, nondecaying oscillations around what is expected to be the saturation value. These oscillations can be explained as a superposition of just a few harmonics that correspond to the shortest periodic orbits in the rectangle. The analytical and numerical results are in excellent agreement.

DOI: 10.1103/PhysRevE.72.056209 PACS number(s): 82.40.Bj, 05.30.−d, 05.90.+m, 02.50.−r

I. INTRODUCTION

Two decades ago Casati, Chirikov, and Guarneri [1] and Berry [2] made numerical and analytical studies of the level statistics in rectangular billiards for large quantum numbers (semiclassical quantization). Casati *et al.* [1] demonstrated numerically that the distribution function of the nearest-neighbor energy level spacings is exponential (obeys the Poisson law [3]), which is generally the case for classically integrable systems and is well understood theoretically [4]. Further, they studied the behavior of the level rigidity [3] in the spectral staircase and showed that, following the initial linear growth with the width of the interval, the rigidity saturates to a constant value. This behavior was explained by Berry [2] who argued that the width of the interval at which the saturation occurs corresponds to the shortest periodic orbit in the billiard and that the saturation value of the rigidity can be obtained as a sum over the periodic orbits. Subsequently, the results of [1] were reproduced with high numerical precision in Refs. [5,6].

In previous work [7], we interpreted this result in terms of global level rigidity and proposed an ansatz for the level density correlation function which described the transition from linear to saturation behavior and which is similar, aside from the energy scale, to counterparts in Gaussian ensembles corresponding to classically chaotic systems [3,4]. The ansatz suggested that the level number variance should exhibit decaying oscillations as the interval increases, approaching a saturation value which according to the integral relation between rigidity and variance [3]—see below—should differ by a factor of 2.

In the present paper, we report numerical calculations which show, surprisingly, that, as the width of the energy interval increases, the variance in level number oscillates without decay—and it is understanding this feature which motivates this work. Excellent agreement with the numerical results is obtained with a level density correlation function derived from the periodic orbits of a semiclassical formulation of the level density [2,4]. In the Appendix A is given a quantum derivation of essentially the same result, which, however, applies to the statistics of energy levels of any separable Hamiltonian.

In contrast with Refs. [5,6], the numerical results presented here are *ensemble averages*, as opposed to averages over an energy interval for a particular rectangular billiard, the ensemble being a fairly large set of rectangles of the same area but a range of ratios L_1/L_2 of the sides. This eliminates sample-specific "noise" as well as other artifacts like the high degeneracies of a square billiard. The importance of the ensemble average is underscored by the fact that the onset of saturation, that is, the width of the energy interval at which the saturation develops and the saturation value itself both depend critically on the position of the interval in the spectrum [2], scaling as the square root of the central energy of the interval. These statistical features are effectively smeared out by averaging over intervals of a single spectrum as in Refs. [5,6]. For instance, while the plot of variance in [5] shows oscillations, they appear to be decaying and irregular and were not recognized as an intrinsic feature.

II. DEFINITIONS OF ENSEMBLE AND STATISTICAL MEASURES: COMPARISON WITH GAUSSIAN ENSEMBLES

We will consider intervals $[\varepsilon-E/2,\varepsilon+E/2]$, $E\ll\varepsilon$, where the states with energies near ε have large quantum numbers and can be described semiclassically. Denote by $\mathcal{N}(\varepsilon)$ the cumulative number of levels (or spectral staircase) [4]

$$\mathcal{N}(\varepsilon)=\sum_k \theta(\varepsilon-\varepsilon_k) \tag{1}$$

where θ is the unit step function and k labels the energy eigenstates. A "universal" representation of the ladder data is obtained by rescaling the energy variable so as to eliminate the particular shape of the average $\langle\mathcal{N}(\varepsilon)\rangle$ from the ladder [4]. To do this, define the new scaled *dimensionless* energy variable ε' by

$$\varepsilon\to\varepsilon'(\varepsilon)\equiv\langle\mathcal{N}(\varepsilon)\rangle. \tag{2}$$

Here $\langle\ \rangle$ denotes the ensemble average. In particular, to a computed eigenvalue ε_k the value $\varepsilon_k'=\langle\mathcal{N}(\varepsilon_k)\rangle$ is assigned. Since ε' is a monotone function of ε

$$\langle \mathcal{N}'(\varepsilon') \rangle = \langle \mathcal{N}(\varepsilon) \rangle = \varepsilon', \tag{3}$$

so that the mean level density is *unity* in the scaled variable

$$\rho'(\varepsilon') = \left\langle \sum_k \delta(\varepsilon' - \varepsilon_k') \right\rangle = 1. \tag{4}$$

Since $\langle \mathcal{N}(\varepsilon) \rangle$ is used as the scaled energy axis variable in order to give the ladders an approximately 45° slope, it is important to have a fair idea of its functional form for presenting the numerical data.

The asymptotic cumulative spectrum $\langle \mathcal{N}(\varepsilon) \rangle$ of eigenvalues of the wave equation in a region with finite boundaries and various boundary conditions (Dirichlet, Neumann, or mixed) is given in several places [8–10]. In particular, for a two-dimensional (2D) simply connected region, the form for the Dirichlet case ($u=0$ on the boundary) is

$$\langle \mathcal{N}(\varepsilon) \rangle = \frac{\varepsilon}{\Delta} - \frac{f}{2\sqrt{\pi}} \left(\frac{\varepsilon}{\Delta} \right)^{1/2} + c + o(1) \tag{5}$$

where

$$\Delta = \frac{2\pi\hbar^2}{mA}, \quad f = \frac{S}{A^{1/2}}, \tag{6}$$

with S the length of the perimeter and A the area. For a rectangle with $L_1 = \alpha^{-1/4} L$ and $L_2 = \alpha^{1/4} L$, so that $A = L^2$ and $f = 2\beta : \beta = (\alpha^{1/4} + \alpha^{-1/4})$. For a smooth boundary $c = 1/6$, while, for a rectangle, $c = 1/4$. Formula (5) is cited in the references above but the derivation of $c = 1/4$ for the rectangle is not easily extracted from them. At the risk of possible repetition, we give a derivation in the Appendix A—which also clarifies the link between the semiclassical and quantum descriptions of the persistent oscillations of the density correlation function observed in the numerical studies reported here. Extension to other integrable (separable) systems is immediate.

Although formula (5), the "Weyl formula," for the *average* level density at large $\mathcal{N}$ is almost the same for smooth and rectangular boundaries, other features of the spectra are substantially different. The classical motion in a billiard with smooth boundary is in general chaotic and the corresponding quantum Hamiltonian is nonseparable while the classical motion in a rectangular billiard is integrable and the quantum Hamiltonian is separable.

For a rectangle, the energy eigenvalues are

$$\varepsilon_{n_1 n_2} = \frac{\pi^2 \hbar^2}{2m} \left(\frac{n_1^2}{L_1^2} + \frac{n_2^2}{L_2^2} \right). \tag{7}$$

As stated earlier, eigenvalue distributions were calculated for rectangles of the same area $A = L_1 L_2 = L^2$ in an ensemble with different values of the ratio $\alpha = L_2^2 / L_1^2$. Numerically, we use algebraic numbers for α to reduce accidental level degeneracies. (We do not use transcendental numbers because they are "too close" to rational [4].)

Since the present work concentrates on the rigidity of the spectrum of the eigenvalues, we will not discuss the distribution of nearest-neighbor level spacings, except to state that our computations [11] are congruent with those of [1,5,6]. For the statistics of large numbers of levels, the following standard measures will be used. The first is the level rigidity Δ_3, defined in [2,3] as the best linear fit to the spectral staircase in the interval $[\varepsilon - E/2, \varepsilon + E/2]$,

$$\Delta_3(\varepsilon; E) = \left\langle \min_{(A,B)} \frac{1}{E} \int_{\varepsilon - E/2}^{\varepsilon + E/2} d\varepsilon [\mathcal{N}(\varepsilon) - A - B\varepsilon]^2 \right\rangle, \tag{8}$$

the explicit form of which is

$$\left\langle \frac{1}{E} \int_{\varepsilon - E/2}^{\varepsilon + E/2} d\varepsilon\, \mathcal{N}^2(\varepsilon) - \frac{1}{E^2} \left(\int_{\varepsilon - E/2}^{\varepsilon + E/2} d\varepsilon\, \mathcal{N}(\varepsilon) \right)^2 - \frac{12}{E^4} \left(\int_{\varepsilon - E/2}^{\varepsilon + E/2} d\varepsilon\, \varepsilon \mathcal{N}(\varepsilon) \right)^2 \right\rangle. \tag{9}$$

Figure 1 shows an example of such a fit. In this and subsequent figures the scaled energy variable (2) is the x-axis coordinate but the prime is omitted.

For the number of levels N on the interval $[\varepsilon - E/2, \varepsilon + E/2]$

$$N(\varepsilon; E) = \mathcal{N}\left(\varepsilon + \frac{E}{2} \right) - \mathcal{N}\left(\varepsilon - \frac{E}{2} \right) \tag{10}$$

the variance

$$\Sigma(\varepsilon; E) = \langle (N - \langle N \rangle)^2 \rangle \tag{11}$$

is another measure of the fluctuations.

We note in passing that even for an ensemble that is large enough to define smooth averages, the mean level density $\langle \rho \rangle$ and the mean level spacing are not numerical inverses because of the fluctuations (11). Consider an interval E small enough so that $N(\varepsilon; E) \propto E$ and $\Sigma(\varepsilon; E) \propto E$. Then, with

$$\langle \rho(\varepsilon) \rangle = \left\langle \frac{N}{E} \right\rangle = \frac{1}{E} \langle N \rangle \tag{12}$$

and

$$\langle \Delta(\varepsilon) \rangle = \left\langle \frac{E}{N} \right\rangle = E \left\langle \frac{1}{N} \right\rangle, \tag{13}$$

we have [11]

$$\langle \rho \rangle \langle \Delta \rangle = 1 + \frac{1}{\langle N \rangle} + O\left(\frac{1}{\langle N \rangle^2} \right). \tag{14}$$

For classically integrable billiards the last equation holds for $E \ll \sqrt{\varepsilon \langle \rho \rangle^{-1}}$ (see below), so that we can neglect the difference between $\langle \Delta \rangle$ and $\langle \rho \rangle^{-1}$ only for sufficiently large intervals $\langle N \rangle \gg 1$. The global mean level spacing is taken as

$$\Delta = \langle \rho \rangle^{-1} \quad \left(\text{or } \frac{2\pi\hbar^2}{mA} \text{ in the original units} \right). \tag{15}$$

We also note that because $\Sigma(\varepsilon; E) \propto E$ up to the scale of $\sqrt{\varepsilon \langle \rho \rangle^{-1}}$, the "differential" level density $\langle \rho(\varepsilon) \rangle = \langle \Sigma_k \delta(\varepsilon - \varepsilon_k) \rangle$ is not well defined *numerically*. In other words, due to the large fluctuations in the number of levels for a small interval E, it can take a prohibitively large number of ensemble samples to evaluate $\langle \rho(\varepsilon) \rangle$ via Eq. (12) with a reasonable precision [11].

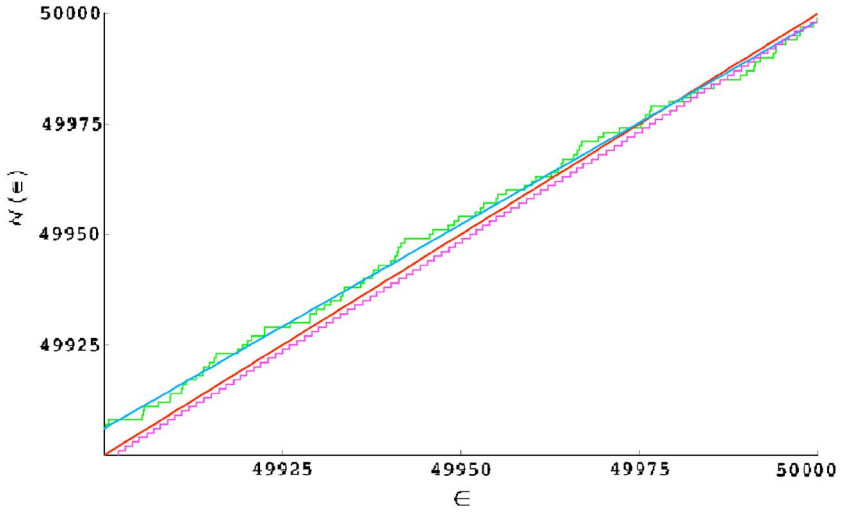

FIG. 1. (Color online) Top straight line and top staircase: best linear fit [unaveraged, single $\alpha=20/109^{3/5}\approx 1.198\,32$, as per inside of $\langle\,\rangle$ in Eq. (8)] of the spectral staircase in the interval $E\in[49\,900,50\,000]$. [We have omitted the primes on ε and E which are understood as, respectively, the renormalized energy variable ε' (2), and the difference between the upper and lower values of ε'.] Bottom straight line and bottom staircase: the 45° slope (3) and the staircase obtained by averaging over 200 staircases corresponding to 200 algebraic α in the [1,2] interval are also presented (notice that these are quite close even for such a small energy interval E; for wider intervals they become indistinguishable to the eye).

The fluctuation measures Σ and Δ_3 can be expressed in terms of the correlation function of the density of levels [3],

$$K(\varepsilon_1,\varepsilon_2)=\langle\delta\rho(\varepsilon_1)\delta\rho(\varepsilon_2)\rangle, \tag{16}$$

$$\delta\rho(\varepsilon)=\rho(\varepsilon)-\langle\rho(\varepsilon)\rangle, \tag{17}$$

regardless of the form of $K(\varepsilon_1,\varepsilon_2)$; for instance,

$$\Sigma(\varepsilon;E)=\int_{\varepsilon-E/2}^{\varepsilon+E/2}\int_{\varepsilon-E/2}^{\varepsilon+E/2}K(\varepsilon_1,\varepsilon_2)d\varepsilon_1 d\varepsilon_2. \tag{18}$$

Using these relationships one can further show that Σ supersedes Δ_3 via an integral relationship [3]

$$\Delta_3(\varepsilon;E)=\frac{2}{E^4}\int_0^E dx(E^3-2xE^2+x^3)\Sigma(\varepsilon,x). \tag{19}$$

For Gaussian ensembles, corresponding to classically chaotic ergodic systems, the functional form of the level correlation function $K(\varepsilon_1,\varepsilon_2)$ is well understood [3]. Denoting

$$\varepsilon=\frac{\varepsilon_1+\varepsilon_2}{2},\quad \omega=\varepsilon_2-\varepsilon_1, \tag{20}$$

it can be written, in most general terms, as

$$K(\varepsilon_1,\varepsilon_2)=K(\omega)=\Delta^{-2}\left[\delta\left(\frac{\omega}{\Delta}\right)-\mathcal{K}\left(\frac{\omega}{\Delta}\right)\right] \tag{21}$$

where

$$\int_{-\infty}^{\infty}\mathcal{K}(x)dx=1 \tag{22}$$

so that

$$\int_{-\infty}^{\infty}K(\omega)d\omega=0. \tag{23}$$

The interpretation of these formulas is as follows. The δ-function term in Eq. (21) describes the correlation of a given level with itself irrespective of other levels. The $\mathcal{K}$ function describes "level repulsion" and has a range of order Δ. The integrals (22) and (23) converge to their values on the scale of $\omega\sim\Delta$ and reflect the fact that an overall "level rigidity" develops on the scale of Δ.

Indeed, by definition of $\delta\rho(\varepsilon)$,

$$\int\delta\rho(\varepsilon)d\varepsilon=0 \tag{24}$$

and thus

$$\int K(\varepsilon_1,\varepsilon_2)d\varepsilon_1=\int K(\varepsilon_1,\varepsilon_2)d\varepsilon_2=0, \tag{25}$$

where integration is over the entire energy spectrum. The integral can be converted to the form (23) when, given a position in the spectrum of the interval center ε, the scale on which the level rigidity (24) develops is much smaller than ε. This behavior is reflected in the forms of Σ,

$$\Sigma(\varepsilon;E)=\begin{cases}\dfrac{E}{\Delta}, & E\lesssim\Delta,\\[2ex] C\ln\left(\dfrac{E}{\Delta}\right), & E\gg\Delta,\end{cases} \tag{26}$$

$$\tag{27}$$

where the constant C depends on the specific Gaussian ensemble [3]. The behavior of Δ_3,

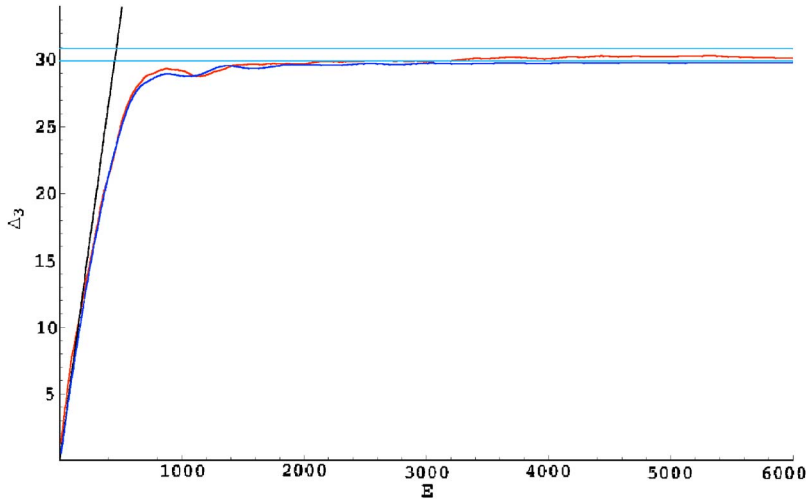

FIG. 2. (Color online) Level rigidity $\Delta_3(\varepsilon;E)$ vs the interval width E for $\varepsilon=10^5$ and 200 algebraic α in the [1,2] interval. The two curves are obtained by numerical evaluation of Δ_3 (slightly higher saturation value) and by substituting the result of numerical evaluation of Σ, shown in Fig. 3, into Eq. (19). The straight line through the origin is $\Delta_3(\varepsilon;E)=E/15$ and corresponds to uncorrelated levels. The two horizontal lines are the saturation ($E \gg E_{\max}$) rigidities Δ_3^∞ calculated from the semiclassical formula (31) for $\alpha=1$ (bottom line) and 2, respectively. (The fact that the curve derived using Σ lies slightly below the theoretical values reflects the somewhat lesser accuracy in the evaluation of Σ.)

$$\Delta_3(\varepsilon;E) = \begin{cases} \dfrac{1}{15}\dfrac{E}{\Delta}, & E \lesssim \Delta, \\ \dfrac{C}{2}\ln\left(\dfrac{E}{\Delta}\right), & E \gg \Delta, \end{cases} \tag{28}$$

(29)

follows from (19). Notice that the linear behavior in Eqs. (26) and (28) originates in the δ-function term in Eq. (21) (uncorrelated levels).

By comparison, for a rectangular box the semiclassical approach describes $\delta\rho(\varepsilon)$ as an oscillatory function in terms of a sum over all periodic orbits [4]. Berry [2] used this approach to obtain the following limiting behaviors of the statistic $\Delta_3(\varepsilon;E)$ for the levels of a single rectangle with ratio α:

$$\Delta_3(\varepsilon;E) = \frac{1}{15}\frac{E}{\Delta}, \quad E \lesssim E_{\max} = (\pi\alpha^{1/2}\varepsilon\Delta)^{1/2}, \tag{30}$$

$$\Delta_3(\varepsilon;E) = \frac{1}{\pi^{5/2}}\left(\frac{\varepsilon}{\Delta}\right)^{1/2} \sum_{M_1=0}^{\infty}\sum_{M_2=0}^{\infty} \frac{\delta_M}{(M_1^2\alpha^{1/2} + M_2^2\alpha^{-1/2})^{3/2}},$$

$$E \gg E_{\max}, \tag{31}$$

$$\to 0.0947\sqrt{\frac{\varepsilon}{\Delta}} \quad \text{for } \alpha \sim 1. \tag{32}$$

Equation (31) gives the saturation rigidity Δ_3^∞, where M_1 and M_2 are the "winding numbers" of the classical periodic orbits [2] and the factor δ_M, defined by

$$\delta_M = \begin{cases} 0 & \text{if } M_1 = M_2 = 0, \\ 1/4 & \text{if one of } M_1 \text{ and } M_2 \text{ is zero}, \\ 1 & \text{otherwise}, \end{cases} \tag{33}$$

differentiates between the self-retracing and non-self-retracing orbits. Notice that both Δ_3^∞ and $E_{\max}$ are functions of the position ε in the spectrum ($\propto\sqrt{\varepsilon}$), which is in contrast with Gaussian ensembles. The quantum scale $E_{\max}$ for the onset of saturation corresponds to the time of traversal of the shortest classical periodic orbit [2],

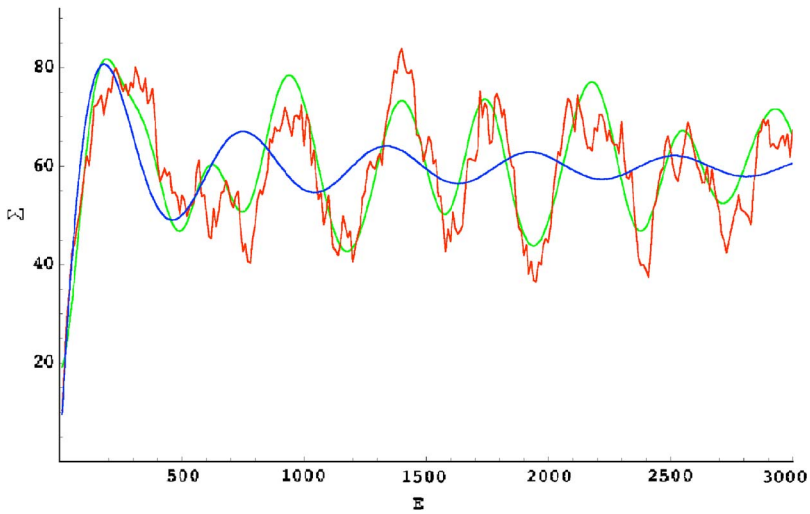

FIG. 3. (Color online) Numerical evaluation of $\Sigma(\varepsilon;E)$ (jagged line) using the same ε and α ensemble as in Fig. 2 (200 algebraic α in the [1,2] interval). The smooth line is the semiclassical theory, Eq. (42), and the decaying wavy curve is the ansatz (35).

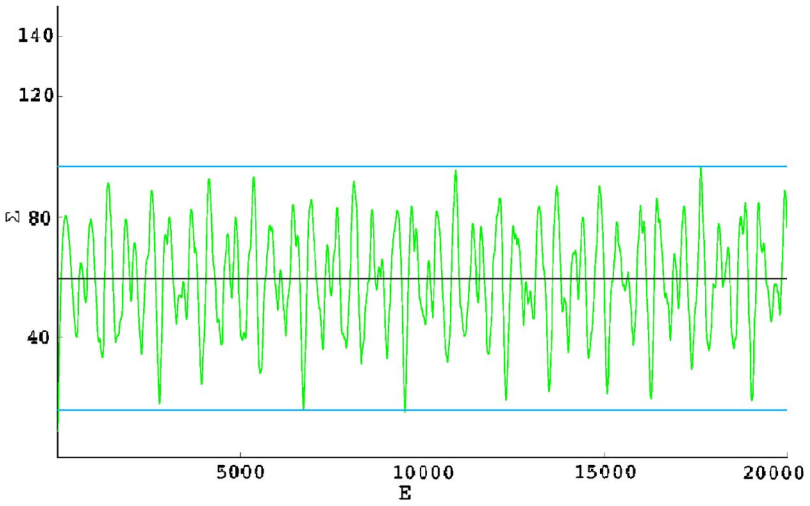

FIG. 4. (Color online) $\Sigma(\varepsilon;E)$ from Eq. (42) for $\varepsilon=10^5$ including 100 harmonics from the single sum and 100 from the double sum.

$$E_{\max} = \frac{h}{T_{\min}}, \tag{34}$$

whose length is just twice the length of the rectangle's smaller side, and the winding numbers are $M_1=0$, $M_2=1$.

The saturation of Δ_3 to Δ_3^∞ in Eqs. (30) and (31) is analogous to but differs significantly from the transition of Δ_3 for a Gaussian ensemble to the weak logarithmic dependence in Eqs. (28) and (29). Consequently, one might expect the level density correlation function for a rectangular box to be similar in form to (21), except that the scale of $\mathcal{K}$ is set by $\sim\sqrt{\varepsilon\Delta}$ instead of Δ. This qualitative reasoning led us earlier [7] to propose the following simple ansatz for K:

$$K(\varepsilon,\omega) = \Delta^{-2}\left[\delta\left(\frac{\omega}{\Delta}\right) - \frac{\Delta}{\pi\omega}\sin\left(\frac{2\pi\omega}{E_{\max}}\right)\right]. \tag{35}$$

This $K(\varepsilon,\omega)$ satisfies Eq. (23) and so is consistent with level rigidity developing on the scale $E_{\max}$. Using this ansatz to evaluate Δ_3 reproduces the saturation to Δ_3^∞ at $E_{\max}$ which is seen in Fig. 2. Equation (35) also predicts the saturation of Σ^∞ to $2\Delta_3^\infty$, but in a damped oscillatory fashion,

$$\frac{\Sigma-\Sigma^\infty}{\Sigma^\infty} = \frac{\sin(E/E_{\max})}{E/E_{\max}}. \tag{36}$$

[This oscillatory behavior is largely washed out in the approach to Δ_3^∞ by the integration in Eq. (19).]

While successfully describing the onset of the level rigidity and of oscillations of Σ on the energy scale of $E_{\max}$, the ansatz (35) does not capture the correct behavior of Σ at larger energies E. The central and rather surprising result of the present work is that the magnitude of the oscillations around Σ^∞ is *not decaying*. This means that there is no precise onset of rigidity at $E\sim E_{\max}$. The oscillatory behavior is shown in the numerical results of Figs. 3–7, and the analysis in Sec. III as well as the Appendix A, supersedes the ansatz (35).

III. CORRELATION FUNCTION OF THE LEVEL DENSITY

In this section we use the semiclassical formulation of the level density $\rho(\varepsilon)$ in which the δ functions are assumed to come from the periodic classical orbits. [A purely quantum mechanical derivation in the Appendix A gives essentially

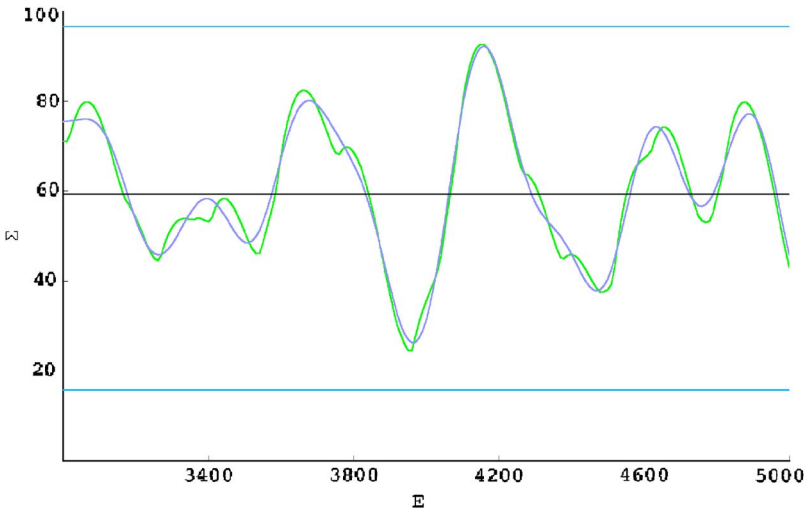

FIG. 5. (Color online) Blown-up section of Fig. 4 compared with a less structured line obtained using a much smaller number of harmonics, namely, three terms each from the single and double sums in Eq. (42). This shows the rapid decrease in higher harmonic amplitude.

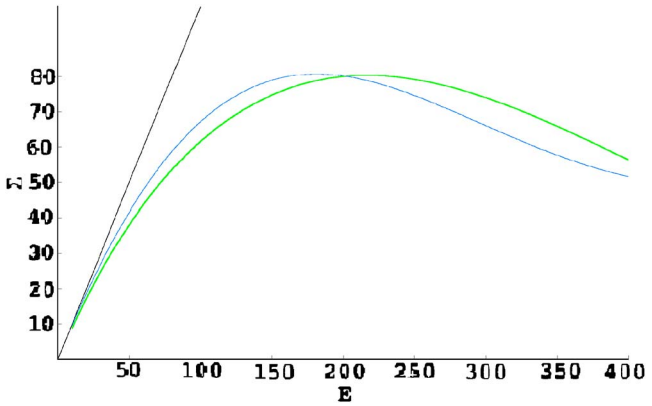

FIG. 6. (Color online) A blowup of the initial part of Fig. 3 for $E \leqslant 400$. The two curves are the ansatz (35) (greater initial slope) and the semiclassical theory (41). The straight line is $\Sigma(\varepsilon;E)=E$, corresponding to uncorrelated levels.

the same $K(\varepsilon,\omega)$; but it also gives the analytical asymptotic form of $\langle N(\varepsilon)\rangle$ which, as stated in Sec. II, is very helpful for a universal representation of the staircase spectrum (and of derived quantities) such as shown in Fig. 1]. From Eqs. (23), (38), (58), and (60) of Berry [2], we obtain the level correlation function as the inverse Fourier transform of Eq. (60), namely,

$$K(\varepsilon,\omega) = \frac{1}{\sqrt{(\pi\Delta)^3\varepsilon}} \sum_{M_1=0}^{\infty} \sum_{M_2=0}^{\infty} 4\delta_M \times \frac{\cos[\sqrt{(4\pi/\varepsilon\Delta)(M_1^2\alpha^{1/2}+M_2^2\alpha^{-1/2})}\,\omega]}{\sqrt{M_1^2\alpha^{1/2}+M_2^2\alpha^{-1/2}}} \tag{37}$$

$$\rightarrow \frac{1}{\sqrt{(\pi\Delta)^3\varepsilon}} \left[4 \sum_{M_1>0}^{\infty} \sum_{M_2>0}^{\infty} \times \frac{\cos[\sqrt{(4\pi/\varepsilon\Delta)(M_1^2+M_2^2)}\,\omega]}{\sqrt{M_1^2+M_2^2}} + 2 \sum_{M>0}^{\infty} \frac{\cos(\sqrt{4\pi/\varepsilon\Delta}M\omega)}{M} \right]_{\alpha\sim 1}. \tag{38}$$

(The energy variables in the above and what follows are now the original dimensional ones.) The paragraph following Eq. (38) in [2] explains the nature of the factor $4\delta_M$ in the above equations; namely, that the factor of 4 is the intensity factor due to constructive interference between the closed orbit and its time-reversed orbit for non-self-retracing orbits when both M_1 and M_2 are nonzero.

For small ω ($\omega \ll \sqrt{\varepsilon\Delta}$) the summation over (M_1,M_2) can be replaced by integration over (x,y) in the entire plane, where

$$x = M_1\alpha^{1/4}\sqrt{\frac{4\pi\Delta}{\varepsilon}}, \quad y = M_2\alpha^{-1/4}\sqrt{\frac{4\pi\Delta}{\varepsilon}}. \tag{39}$$

Converting Eq. (38) into polar coordinates gives

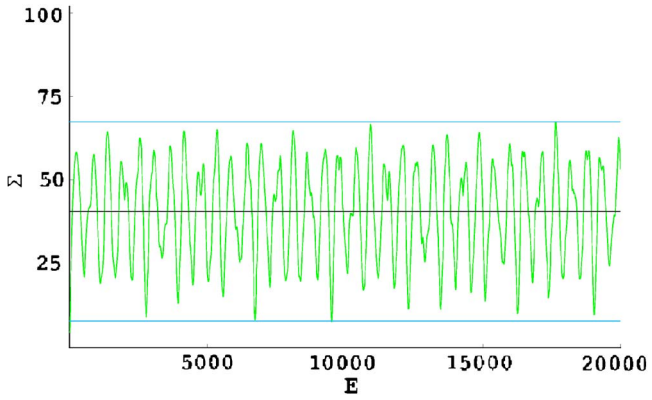

FIG. 7. (Color online) $\Sigma(\varepsilon;E)$ for $\varepsilon=10^5$ for the case of broken time-reversal symmetry, using Eq. (42) but with the modified δ'_M in Eq. (47).

$$K(\varepsilon,\omega) \rightarrow \frac{1}{2\pi^2\Delta^2}\int_0^{2\pi} d\phi \int_0^{\infty} d\rho \cos\left(\frac{\omega}{\Delta}\rho\right) = \Delta^{-2}\delta\left(\frac{\omega}{\Delta}\right) \tag{40}$$

which is just the first term in Eq. (35). Notice, however, that the lower limit of the ρ integral should not extend to zero since $M_{1,2}$ cannot be zero simultaneously. The second term (level repulsion) in Eq. (35) is obtained, following [7], by choosing the lower cutoff in the ρ integral at $\rho_{\min}=y_{\min}=\alpha^{-1/4}\sqrt{4\pi\Delta/\varepsilon}$.

In the opposite case, $\omega \ll \sqrt{\varepsilon\Delta}$, the terms in the series (37) become rapidly oscillating with amplitude and also rapidly decreasing with increase of the winding numbers $M_{1,2}$. Consequently, the sum is dominated by just a few terms with the smallest $M_{1,2}$, and these are responsible for the *nondecaying oscillations* of Σ which are discussed below.

IV. LEVEL NUMBER VARIANCE

Combining Eqs. (18) and (37), we find [on replacing the variable $(\varepsilon_1+\varepsilon_2)/2$ by its central value in the interval]

$$\Sigma(\varepsilon;E) = \sqrt{\frac{\varepsilon}{\pi^5\Delta}} \sum_{M_1=0}^{\infty} \sum_{M_2=0}^{\infty} 4\delta_M \times \frac{\sin^2[E\sqrt{(\pi/\varepsilon\Delta)(M_1^2\alpha^{1/2}+M_2^2\alpha^{-1/2})}]}{(M_1^2\alpha^{1/2}+M_2^2\alpha^{-1/2})^{3/2}} \tag{41}$$

$$\rightarrow \sqrt{\frac{\varepsilon}{\pi^5\Delta}} \left[4 \sum_{M_1>0}^{\infty} \sum_{M_2>0}^{\infty} \frac{\sin^2[E\sqrt{(\pi/\varepsilon\Delta)(M_1^2+M_2^2)}]}{(M_1^2+M_2^2)^{3/2}} + 2 \sum_{M>0}^{\infty} \frac{\sin^2(E\sqrt{\pi/\varepsilon\Delta}M)}{M^3} \right]_{\alpha\sim 1}. \tag{42}$$

For narrow intervals, Eq. (41) reduces to

$$\Sigma(\varepsilon;E) = \frac{E}{\Delta}, \quad E \ll E_{\max}, \tag{43}$$

which follows either from Eqs. (18) and (40) or directly from Eq. (41) if summation is replaced with integration using the

variables (39). It is also consistent with Eqs. (19) and (30).

Figure 3 shows the result of evaluation of Σ using Eq. (41) (with the upper limit of summation on $M_{1,2}$ limited to 100) versus the numerical evaluation of Σ for the ensemble of 200 algebraic α's $\in[1,2]$. We also show Σ obtained using the ansatz (35) of Ref. [7]. Clearly, the latter adequately describes the transition from the small-scale $E \ll E_{\max}$ linear behavior (43) to scales of $E \sim E_{\max}$, but fails to describe the large-scale behavior, $E \gg E_{\max}$. On the other hand, the agreement of numerical evaluation with the theoretical result (41) for all E is quite remarkable.

Two comments are in order. First, it was necessary to have a sufficient spread of α values (between 1 and 2 here) to obtain reliable statistics for large quantum numbers from our relatively small α ensembles (200 values here). However, the dependence on α of the relevant parameters is quite weak, through $\alpha^{\pm 1/4}$, so that, for $\alpha \in [1,2]$, the difference from an ensemble with α values close to 1 is not significant. Second, for $E \gg E_{\max}$ it is sufficient to limit summation on $M_{1,2}$ to 2 and 3 in the double and single sum, respectively, to obtain a curve that is very close to the full theoretical curve. As was explained above, this is because the amplitudes of the quickly oscillating terms in the sum rapidly fall off with increasing $M_{1,2}$.

We now turn to the theoretical curve in Fig. 4 that represents the level number variance given by (42) including up to 400 harmonics. The α-ensemble values are now close to 1. Figure 5 shows how well the variance is reproduced by the superposition of only six harmonics: three from the double sum and three (with commensurate frequencies) from the single sum. These are nondecaying oscillations whose amplitude is given by

$$\frac{\Sigma^{+}}{\Sigma^{\infty}} \approx 0.63, \quad \frac{\Sigma^{-}}{\Sigma^{\infty}} \approx 0.74, \tag{44}$$

where $\Sigma^{+}=\max\{\Sigma\}-\Sigma^{\infty}$, $\Sigma^{-}=\Sigma^{\infty}-\min\{\Sigma\}$, and Σ^{∞} is the mean value of oscillating Σ obtained by substituting $\sin^2 \to 1/2$ in Eq. (41). The asymmetry of the positive and negative swings of Σ oscillations, $\Sigma^{+} \neq \Sigma^{-}$, is due to the asymmetry of the Clausen function [13] $f_{\mathrm{Cl}_3}(x)$, which comes mainly from $k \leqslant 3$

$$f_{\mathrm{Cl}_3}(x) = \sum_{k=1}^{\infty} \frac{\cos kx}{k^3};$$

$\max\{f_{\mathrm{Cl}_3}(x)\}/\min\{f_{\mathrm{Cl}_3}(x)\} \approx 1.3$. This function originates in the single sum in Eq. (42), which corresponds to self-retracing orbits.

Figure 6 illustrates the initial behavior of the curve in Fig. 4. Notably, in this range it is well approximated by the curve generated using the ansatz (35).

It is important to point out that if one averages over the range of α values, or over the range of ε values as in Ref. [5], the beats that result from a superposition of a continuous range of harmonics will present themselves, over relevant interval widths, as decaying oscillations. This is due to the corresponding continuous range of the beat frequencies represented by their envelopes. (A slightly more detailed discussion is given in Appendix B.)

We now turn to breaking of time-reversal symmetry, as for charged particles due to a magnetic field. Clearly, the condition for the latter is given by

$$BA \sim \phi_0 \tag{45}$$

where $\phi_0 = hc/e$ is the flux quantum. For such fields, the Larmor radius is much greater than either side of the rectangle,

$$R = \frac{mcv}{eB} \sim \sqrt{A}\sqrt{\frac{\varepsilon}{\Delta}}, \tag{46}$$

where $mv^2/2 = \varepsilon$. Therefore, the deviation from the free specular scattering will be small and we can find both the level correlation function and the level number variance via simple substitution:

$$\delta_M \to \delta'_M = \begin{cases} 0 & \text{if } M_1 = M_2 = 0, \\ 1/4 & \text{if one of } M_1 \text{ and } M_2 \text{ is zero}, \\ 1/2 & \text{otherwise}, \end{cases} \tag{47}$$

in Eqs. (37) and (41). For the $\alpha \simeq 1$ ensemble considered above, Σ' is shown in Fig. 7. In this case

$$\frac{\Sigma'^{\infty}}{\Sigma^{\infty}} \approx 0.69, \tag{48}$$

$$\frac{\Sigma'^{+}}{\Sigma'^{\infty}} \approx 0.66, \quad \frac{\Sigma'^{-}}{\Sigma'^{\infty}} \approx 0.80. \tag{49}$$

The increased asymmetry of Σ oscillations underscores the increased relative contribution of the single sum to Σ in Eq. (42) (self-retracing orbits).

V. DISCUSSION

The central results of this work are summarized by Figs. 3–7. The first of these graphs shows that the numerical evaluation of the level number variance for a particle in a rectangular box is in excellent agreement with the theoretical result given by Eq. (41). The second indicates a nondecaying oscillatory behavior of Σ. Fig. 7 shows Σ when the time-reversal symmetry is broken. Figures 3 and 4 can be successfully reproduced with just a small number of lowest harmonics in (42), as seen in Fig. 5.

It is remarkable that, for the center of the interval $\varepsilon \gg N\Delta$, $\Sigma(\varepsilon; E)$ exhibits large, reproducible oscillations as a function of the interval width E. The main implication of this result is that while the level rigidity saturation indeed develops on the scale set by $\sim\sqrt{\varepsilon\Delta} \ll \varepsilon$, it is accurate only in an approximation where a harmonic is replaced by its average, namely, zero. In other words, Eq. (23) converges to zero on the scale of $\omega \sim \sqrt{\varepsilon\Delta}$ only up to a sum of harmonic terms, as implied by Eq. (37).

The Σ oscillations are, nonetheless, entirely consistent with the near straight line saturation of Δ_3. Δ_3 does also

exhibit oscillatory behavior around Δ_3^∞, but the oscillatory behavior is both parametrically small in Δ/ε and decays as a function of E. This reduction of Δ_3 can be traced, for instance, to integration in Eq. (19). From the treatment in the Appendix, which essentially reproduces the expression (37) for $K(\varepsilon,\omega)$, it is clear that the basic and general feature behind the oscillatory behavior of $K(\varepsilon,\omega)$ and $\Sigma(\varepsilon,\omega)$ is the separability of the Hamiltonian. This leads to two sets of integral quantum numbers which can always be arranged on a lattice and define persistent Fourier components which dominate when N is very large.

VI. SUMMARY

We investigated the oscillatory behavior of the level number variance Σ in a rectangular box.

Analytically, Σ is obtained from the level density correlation function (37) and is given by Eq. (41). Physically, it is a manifestation of the long-range correlations in the level density. Semiclassically, while the individual levels are obtained by Born-Sommerfeld quantization of action variables, the scale of level correlations is determined by the periodic orbits [4]. Relative to Ref. [2], our contribution is as follows: Obtaining the real space version of the level correlation function Eq. (37), which then results in Eq. (41); emphasizing Σ, rather than Δ_3, as a better indicator of long-range correlations in the level density; showing that the initial rise and approach to saturation can be described by Eq. (35); showing that the oscillations around the saturation value can be described by the few first harmonics of the infinite sum (41); and deriving Eq. (37) directly from quantum mechanics, along the lines of Ref. [12], without using semiclassical formalism.

Numerically, we studied the oscillations of Σ using ensemble averaging, as opposed to the more common energy averaging [5,6]. This is the usual method in mesoscopic physics, where ensembles corresponds to different realizations of disorder in otherwise like systems. In the rectangle, we define ensemble in terms of the aspect ratio α of the rectangle sides (α ensemble). For numerical verification of the oscillations of Σ it is important to keep α's close to a fixed value; otherwise, since the frequency depends on α, adding harmonics with varied frequencies will result in beats that appear as decaying oscillations. (As explained in Appendix B, the energy dependence of frequency is stronger than the α dependence, suggesting that energy averaging is more likely to result in beats "masquerading" as decaying oscillations; while we believe this might have been the case in Ref. [5], where the oscillations of Σ were first observed numerically, we hope to investigate this issue in a more thorough fashion in a separate work.) However, if the α's are kept close, one needs to exercise care in order to have a representative sampling. The narrower the range of α's and the larger the number of α's per given range, the higher in spectrum the center of the interval needs to be (larger quantum numbers) to attain it. The effectiveness of our technique is confirmed by the following observations: α-ensemble averaging of individual staircases, shown in Fig. 1, results in a straight line with a 45° slope; given the center of the interval and the range of α's that we used, the positions of the levels and the corresponding pairs of quantum numbers showed no significant correlations between various α's; and numerical averaging greatly improves with the increase of the number of α's used until such number becomes sufficiently large; its further increase leads to a slow approach of quantities to the values consistent with theoretical predictions.

In the future, we will investigate the level number variance in a variety of finite-domain and potential problems. We will also address the explicit dependence of the level correlation function on the magnetic field for a detailed description of the time-reversal breaking transition and to address the orbital magnetism of nonresonant integrable systems.

Note added. Recently, we received a communication from Marklof pointing our attention to Refs. [14,15]. In particular, the nondecaying oscillatory behavior of the level number variance that we observe in the present paper seems to be in correspondence with the behavior of the scaling function $V(z)$ in Ref. [14].

ACKNOWLEDGMENT

We wish to thank Richard Gass for his extensive help with MATHEMATICA.

APPENDIX A: QUANTUM MECHANICAL DERIVATION OF THE DENSITY OF STATES

This is an extension (independently derived) of von Oppen's application of the Poisson summation method to the *square* billiard [12]. It illuminates the basic difference between quantum mechanically separable (classically integrable) and nonseparable (chaotic) Hamiltonians. For motion in 2D a separable Hamiltonian has two quantum numbers—which are discrete for the confined motion in billiards but also for motions like the Coulomb bound states, which are not strictly confined. Equation (7) contains two integers n, m which lie inside the first quadrant of a 2D square lattice with unit spacing. The "perturbed" Coulomb problem, $V(r)=-\alpha r^{-1}+\beta r^{-2}$, α, $\beta>0$, is separable in r and θ; and the quantum numbers n_r, m ($\equiv l$) form a lattice subset, $n_r=0, 1, 2, \ldots$, $m=0, \pm1, \pm2, \ldots$.[1]

For a rectangular box, let $\mathbf{k}$ be a continuous vector in the space with the integer lattice points $\mathbf{k_m}=(m_1,m_2)$. The density of states in $\mathbf{k}$ space is

$$\rho(\mathbf{k})=\sum_{\text{allowed } \mathbf{m}} \delta^{(2)}(\mathbf{k}-\mathbf{k_m}). \tag{A1}$$

According to Eq. (7) $\varepsilon(-\mathbf{k_m})=\varepsilon(\mathbf{k_m})$, so we can extend Eq. (A1) to include all $\mathbf{m}$. Multiple counting is avoided by writing

$$\rho(\mathbf{k})=(1/4)\{\Delta^{(2)}(\mathbf{k})-\Delta^{(1)}(k_x)\delta(k_y)-\Delta^{(1)}(k_y)\delta(k_x)+\delta^{(2)}(\mathbf{k})\} \tag{A2}$$

where $\Delta^{(1,2)}$ are the lattice δ functions:

[1] We hope to discuss the perturbed Coulomb problem in a separate publication [16].

$$\Delta^{(1)}(k)=\sum_{m=-\infty}^{\infty}\delta(k-m),\quad \Delta^{(2)}(\mathbf{k})=\sum_{\text{all }\mathbf{m}}\delta^{(2)}(\mathbf{k}-\mathbf{m}). \tag{A3}$$

The Poisson-sum representation of Eq. (A3) is

$$\Delta^{(1)}(k)=\sum_{\nu=-\infty}^{\infty}e^{iw_\nu k},\quad \Delta^{(2)}(\mathbf{k})=\sum_{\text{all }\nu}e^{i\mathbf{w}_\nu\cdot\mathbf{k}} \tag{A4}$$

where

$$w_\nu=2\pi\nu,\quad \mathbf{w}_\nu=2\pi(\nu_1,\nu_2) \tag{A5}$$

and the ν's are integers. Equations (A2)–(A5) restate $\rho(\mathbf{k})$ as a discrete Fourier series. Let $\phi(\mathbf{k})$ be a continuous function with

$$\phi(\mathbf{k}_\mathbf{m})=\varepsilon(m_1,m_2). \tag{A6}$$

The interpolation function $\phi(\mathbf{k})$ is not unique in general and the functions $I_\nu(\varepsilon)$ introduced in Eq. (A9) below will depend on the choice of ϕ. However, the sum over all ν contains only $\delta^{(2)}(\mathbf{k}-\mathbf{m})$ and is unique. Here we choose the "simplest" $\phi(\mathbf{k})$, namely, replacing (m_1,m_2) in $\varepsilon(m_1,m_2)$ by (k_x,k_y).

The density of states in the variable ε is

$$\rho(\varepsilon)=\sum_{\text{allowed }\mathbf{m}}\delta(\varepsilon-\varepsilon(\mathbf{m}))=\int d^2k\;\delta(\varepsilon-\phi(\mathbf{k}))\rho(\mathbf{k}). \tag{A7}$$

Inserting the form of $\rho(\mathbf{k})$ from Eqs. (A2)–(A4) gives

$$\rho(\varepsilon)=\rho^{(2)}(\varepsilon)+\rho^{(1)}(\varepsilon)+\frac{1}{4}\delta(\varepsilon-\varepsilon(\mathbf{k}=\mathbf{0})). \tag{A8}$$

A typical Fourier component of $\Delta^{(2)}(\mathbf{k})$ involves the k integral

$$I_\nu(\varepsilon)=\frac{1}{4}\int d^2k\;\delta(\varepsilon-\phi(\mathbf{k}))e^{i\mathbf{w}_\nu\cdot\mathbf{k}}. \tag{A9}$$

Now define L_ε to be the (level) line of constant $\phi(\mathbf{k})$: $\phi(\mathbf{k})=\varepsilon$, and let $k_\parallel,k_\perp$ be tangential and perpendicular local coordinates along L_ε. Then

$$I_\nu(\varepsilon)=\frac{1}{4}\int_{L_\varepsilon}dk_\parallel\frac{1}{|\nabla_k\phi|}e^{i\mathbf{w}_\nu\cdot\mathbf{k}}. \tag{A10}$$

We first check this procedure for a *square box* retaining *only* the $\rho^{(2)}(\varepsilon)$ terms—as did von Oppen [12]. Here $\phi(\mathbf{k})=ck^2$, where $c=\pi^2\hbar^2/2mL^2=\Delta$ in dimensional units (or 1/4 in dimensionless units). Then $|\nabla_k\phi|=2ck$ and L_ε is a circle of radius $k=\sqrt{\varepsilon/c}$, so that

$$I_\nu(\varepsilon)=\frac{1}{8c}\int d\theta\,e^{iw_\nu k\cos(\theta)}=\frac{\pi}{4c}J_0(w_\nu k), \tag{A11}$$

giving

$$\rho^{(2)}(\varepsilon)=(1\text{ or }\Delta^{-1})\sum_{\text{all }\nu}J_0(w_\nu k) \tag{A12}$$

This agrees with von Oppen's Eq. (B4) [12].

We now turn to the *rectangular box*. Equation (7) reads $\phi(\mathbf{k})=c(\alpha^{1/2}k_x^2+\alpha^{-1/2}k_y^2)$ and L_ε is an ellipse—which becomes a circle of the same area in the new coordinates: $\tilde{k}_{x,y}=\alpha^{\pm1/4}k_{x,y}$. $\phi(\mathbf{k})$ simplifies to $c\tilde{k}^2$ and $\mathbf{w}_\nu\cdot\mathbf{k}=\tilde{\mathbf{w}}_\nu\cdot\tilde{\mathbf{k}}$ where $\tilde{\mathbf{w}}_\nu=2\pi(\alpha^{-1/4}\nu_1,\alpha^{1/4}\nu_2)$. Since the Jacobian of the transformation is unity, we can write immediately

$$\rho^{(2)}(\varepsilon)=\sum_{\text{all }\nu}J_0[\tilde{w}_\nu\tilde{k}(\varepsilon)]. \tag{A13}$$

To find $\rho^{(1)}(\varepsilon)$ consider a single $\Delta^{(1)}(k_x)$ term in Eqs. (A2) and (A4). Corresponding to the 2D expression for a single k term in Eq. (A9), we get here

$$-\frac{1}{4}\int dk_x\delta(\varepsilon-c\alpha^{1/2}k_x^2)e^{iw_\nu k_x}=-\frac{\alpha^{-1/4}}{2\sqrt{\pi\varepsilon}}\cos[w_\nu k_x(\varepsilon)], \tag{A14}$$

$$k_x(\varepsilon)=2\alpha^{-1/4}(\varepsilon/\pi)^{1/2}.$$

For $\Delta^{(1)}(k_y)$ replace α by α^{-1}, getting in dimensionless units

$$\rho^{(1)}(\varepsilon)=-\frac{1}{2\sqrt{\pi\varepsilon}}\sum_{\nu=-\infty}^{\infty}\{\alpha^{-1/4}\cos[w_\nu k_x(\varepsilon)]+\alpha^{1/4}\cos[w_\nu k_y(\varepsilon)]\}. \tag{A15}$$

Finally, the term $\delta^{(2)}(\mathbf{k})$ in Eq. (A2) gives

$$\frac{1}{4}\delta(\varepsilon-\phi(\mathbf{0}))=\frac{1}{4}\delta(\varepsilon). \tag{A16}$$

Since $k(\varepsilon)\sim\varepsilon^{1/2}\sim\mathcal{N}^{1/2}$, where $\mathcal{N}$ is the number of levels below ε, and $|\mathbf{w}_\nu|\sim2\pi\nu$ (or $|\nu|$), the arguments of the oscillatory functions in Eqs. (A13) and (A15) are large for large $\mathcal{N}$ so that, except for $\nu=0$, these functions oscillate rapidly around zero with period of order $\nu^{-1}\mathcal{N}^{1/2}$, i.e., more rapidly for larger ν. It is natural to define the mean value $\bar{\rho}(\varepsilon)$ as being the contribution of the $\nu=0$ Fourier components. Then

$$\bar{\rho}(\varepsilon)=1-\frac{\beta}{\sqrt{\pi\varepsilon}}+\frac{1}{4}\delta(\varepsilon) \tag{A17}$$

which, when integrated, gives Eq. (5). (In the deformation ensemble β is replaced by $\langle\beta\rangle$.)

The level density fluctuation is given by the nonzero Fourier components in Eqs. (A13) and (A15), so the level density correlation function (16) is determined by their products. Only products like $\cos[w_\nu k_x(\varepsilon)]\cos[w_\nu k_y(\varepsilon')]$ with the same magnitude $|\mathbf{w}_\nu|$ will produce the "systematic" dependence on the energy *difference* displayed in Eqs. (37) and (38). The other products give oscillatory terms with arguments ε, ε', $\varepsilon+\varepsilon'\gg\omega$ and lead to rapid randomlike contributions. These latter may be responsible for the difference between the numerical and analytic results seen in Fig. 3 (the red and green lines, respectively).

If we retain only $\rho^{(2)}(\varepsilon)$, namely, the full lattice sum in Eq. (A2), we get the semiclassical form for $K(\varepsilon,\omega)$ of

Eq. (37). $\rho^{(1)}(\varepsilon)$, the sum from points on the x and y axes, adds coherently to the axes Fourier terms of $\rho^{(2)}(\varepsilon)$. Thus, $\rho^{(1)}(\varepsilon)$ is apparently not contained in the semiclassical sum (37). This has the effect that $\delta_{\mathbf{m}}$ should be modified for $\mathbf{m}=(m,0)$ and $(0,m)$ by an amount proportional to $\nu\varepsilon^{-1/4}$. For small ν (or m) and $\varepsilon \sim 10^{4-5}$, as in Figs. 3–7, this is a small correction.

APPENDIX B: PERIODIC ORBIT REPRESENTATION OF LEVEL NUMBER VARIANCE

This contains a more general semiclassical representation of level number variance, decoupled from a specific form of the integrable confining potential. According to Berry [2], the saturation rigidity is given by

$$\Delta_3^{\infty}(\varepsilon;E) = \frac{2}{\hbar^{N-1}} \sum_j \frac{A_j^2}{T_j^2} \tag{B1}$$

where A_j and T_j are the amplitudes and the periods of the periodic orbits and $2N$ is the dimension of phase space. For a rectangle, A_j and T_j are explicitly evaluated in Ref. [2] and yield Eqs. (31) and (32).

In the same limit $E \gg E_{\max} \sim \hbar/T_{\min}$, where $T_{\min}$ is the period of the shortest periodic orbit, and using the same formalism, the leading term for the level number variance can be shown to be

$$\Sigma^{\infty}(\varepsilon;E) = \frac{8}{\hbar^{N-1}} \sum_j \frac{A_j^2}{T_j^2} \sin^2\left(\frac{ET_j}{2\hbar}\right). \tag{B2}$$

Averaging over the oscillations, we find

$$\bar{\Sigma}^{\infty}(\varepsilon;E) = \frac{4}{\hbar^{N-1}} \sum_j \frac{A_j^2}{T_j^2} = 2\Delta_3^{\infty}. \tag{B3}$$

Note that A_j and T_j depend explicitly on the position of the center of the interval $\varepsilon \gg E$, the width of the interval. In a rectangle, for instance,

$$T_j = 2\hbar \sqrt{\frac{\pi}{\varepsilon\Delta}(M_1^2\alpha^{1/2} + M_2^2\alpha^{-1/2})}, \quad j = \{M_1, M_2\},$$

determines the periods of oscillations due to $\sin^2(ET_j/2\hbar)$ in Eq. (B2) [compare with Eq. (41)].

We note that the corrections to Δ_3^{∞} also exhibit oscillatory behavior which can be derived analytically either directly from Berry's evaluation or via substitution of Eq. (B2) into Eq. (19). In contrast to Σ^{∞}, however, the amplitude of these oscillations is small in the parameter $E_{\max}/E \sim \hbar/ET_{\min}$. Numerically, the small decaying oscillations on approach to Δ_3^{∞} are observed in Fig. 2.

The above result for Σ^{∞} is an average so that numerically averaging must be performed in order to verify it. Previous authors [5,6] used the spectral averages (averages over ε) which resulted in mixing of harmonics in Eq. (B2). As a result, while the oscillations of Σ^{∞} were indeed observed, they appeared as decaying for the interval widths E studied there. We used ensemble averaging over α, keeping $\alpha^{1/4}$, the parameter on which the energy and time scales depend in the problem, close to 1 as to avoid such mixing. As seen from Figs. 2 and 3, our results are in excellent agreement with theory.

[1] G. Casati, B. V. Chirikov, and I. Guarneri, Phys. Rev. Lett. **54**, 1350 (1985).
[2] M. V. Berry, Proc. R. Soc. London, Ser. A **400**, 229 (1985).
[3] T. A. Brody, J. Flores, J. B. French, P. A. Mello, A. Pandey, and S. S. M. Wong, Rev. Mod. Phys. **53**, 385 (1981).
[4] Martin C. Gutzwiller, *Chaos in Classical and Quantum Mechanics* (Springer-Verlag, New York, 1990).
[5] C. Grosche, *Emerging Applications of Number Theory* (Springer-Verlag, New York, 1999).
[6] M. Robnik and G. Veble, Prog. Theor. Phys. Suppl. **139**, 544 (2000); see also J. Phys. A **31**, 4669 (1998).
[7] R. A. Serota and J. M. A. S. P. Wickramasinghe, Int. J. Mod. Phys. B **16**, 4649 (2002).
[8] R. B. Balian and C. Bloch, Ann. Phys. (N.Y.) **60**, 401 (1970).
[9] M. Kac, Am. Math. Monthly **93**, 1 (1966).
[10] H. P. Baltes and E. R. Hilf, *Spectra of Finite Systems* (Bibliographisches Institut, Mannheim, 1976).
[11] J. M. A. S. P. Wickramasinghe, R. A. Serota, and B. Goodman (unpublished).
[12] Felix von Oppen, Phys. Rev. B **50**, 17151 (1994).
[13] L. Lewin, *Dilogarithms and Associated Functions* (Macdonald, London, 1958); Eric W. Weisstein, http://mathworld.wolfram.com/ClausenFunction.html
[14] P. M. Bleher and J. L. Lebowitz, J. Stat. Phys. **74**, 167 (1993).
[15] J. Marklof, Commun. Math. Phys. **199**, 169 (1998).
[16] J. M. A. S. P. Wickramasinghe, B. Goodman, and R. A. Serota (unpublished).